

Cite this: *RSC Med. Chem.*, 2025, 16, 3495

Discovery of PZ671, a highly potent and *in vivo* active CRBN-recruiting Bcl-xL degrader†

Peiyi Zhang,^{‡a} Dinesh Thummuri,^{‡b} Wanyi Hu,^a Sajid Khan,^b Yonghan He,^b Xuan Zhang,^a Pratik Pal,^a Dongwen Lv,^b Daohong Zhou^{*bc} and Guangrong Zheng^{iD *a}

The conversion of conventional inhibitors of Bcl-xL, a key anti-apoptotic protein, to PROTAC degraders has shown significant promise, particularly in mitigating the on-target thrombocytopenia associated with Bcl-xL inhibition but improving their potency. Previously, we reported XZ739, a CRBN-recruiting Bcl-xL PROTAC that was 20-fold more potent than its parent inhibitor ABT-263 against Bcl-xL-dependent MOLT-4 cells while reducing toxicity to human platelets. Building on XZ739, we here report the discovery of PZ671, a more potent Bcl-xL degrader with ~10-fold improved cellular activity against MOLT-4 cells ($IC_{50} = 1.3$ nM) and ~6-fold enhanced degradation potency against Bcl-xL ($DC_{50} = 0.9$ nM) as well as superior potency across multiple SCLC cell lines compared to XZ739. *In vivo* studies revealed that PZ671 could effectively inhibit MOLT-4 xenograft growth in mice but caused only a moderate and transient reduction in platelet counts following its administration. Our findings highlight the potential of CRBN-recruiting Bcl-xL degraders as promising anticancer agents with improved efficacy and manageable platelet toxicity.

Received 7th February 2025,
Accepted 15th May 2025

DOI: 10.1039/d5md00119f

rsc.li/medchem

Introduction

Apoptosis, a programmed cell death process, is fundamental for maintaining tissue homeostasis and eliminating damaged or unnecessary cells.¹ Dysregulation of apoptosis is a hallmark of cancer, enabling malignant cells to evade death signals and proliferate uncontrollably.² Targeting the apoptotic machinery has thus emerged as a promising strategy in cancer therapy. The B-cell lymphoma 2 (Bcl-2) protein family plays a central role in regulating apoptosis. This family consists of pro-apoptotic (*e.g.*, BAX, BAK) and anti-apoptotic (*e.g.*, Bcl-2, Bcl-xL, Mcl-1) proteins, which collectively govern mitochondrial integrity and caspase activation. Anti-apoptotic proteins, notably Bcl-2, Bcl-xL, and Mcl-1, are frequently overexpressed in cancers, conferring a survival advantage to malignant cells.^{3–7} Among them, Bcl-xL is the most frequently overexpressed protein in solid tumors

and a subset of leukemias and lymphomas.⁸ Tumor resistance to anticancer therapies has also been found to be positively correlated with Bcl-xL expression.⁹ Our recent studies revealed that Bcl-xL inhibitors also possess senolytic properties, enabling the selective elimination of senescent cells implicated in aging and age-related diseases.^{10–12} This dual activity renders Bcl-xL a target with broader therapeutic implications beyond cancer treatment.

Over the past two decades, numerous Bcl-xL selective or Bcl-xL/Bcl-2 dual inhibitors have been developed (Fig. 1).¹³ Early efforts in targeting the Bcl-2 family led to the development of ABT-737, the first potent Bcl-xL/Bcl-2 dual inhibitor developed *via* fragment-based drug discovery by NMR approach.^{14,15} ABT-737 served as a prototype for subsequent Bcl-xL/Bcl-2 dual inhibitors, such as navitoclax (ABT-263), which is orally bioavailable and has been in phase II clinical trials for hematological malignancies and small cell lung cancer (SCLC).¹⁶ However, these inhibitors caused dose-limiting thrombocytopenia due to Bcl-xL's role in platelet survival, which cannot be solved by conventional medicinal chemistry, greatly limiting their clinical utility.

Efforts to mitigate the on-target platelet toxicity associated with Bcl-xL inhibition have driven the exploration of innovative strategies, including prodrugs,¹⁷ antibody–drug conjugates (ADCs),¹⁸ and proteolysis-targeting chimeras (PROTACs) (Fig. 2).^{13,19–28} PROTACs utilize E3 ligases to induce targeted protein degradation, offering the potential for

^a Department of Medicinal Chemistry, College of Pharmacy, University of Florida, Gainesville, FL, 32610, USA. E-mail: zheng@cop.ufl.edu

^b Department of Pharmacodynamics, College of Pharmacy, University of Florida, Gainesville, FL, 32610, USA. E-mail: zhou@uthscsa.edu

^c Department of Biochemistry and Structural Biology, Center for Innovative Drug Discovery, University of Texas Health Science Center at San Antonio, San Antonio, TX, 78229, USA. E-mail: zhou@uthscsa.edu

† Electronic supplementary information (ESI) available. See DOI: <https://doi.org/10.1039/d5md00119f>

‡ Equal contribution as first author to this work.



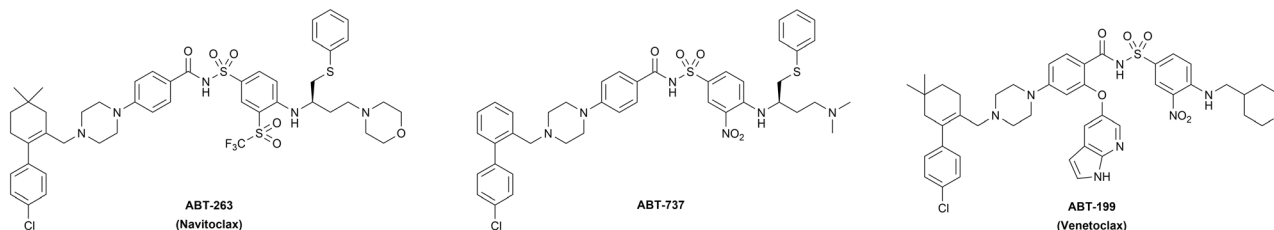


Fig. 1 Structures of representative Bcl-xL/Bcl-2 dual (ABT-263 and ABT-737) and Bcl-2 selective (ABT-199) inhibitors.

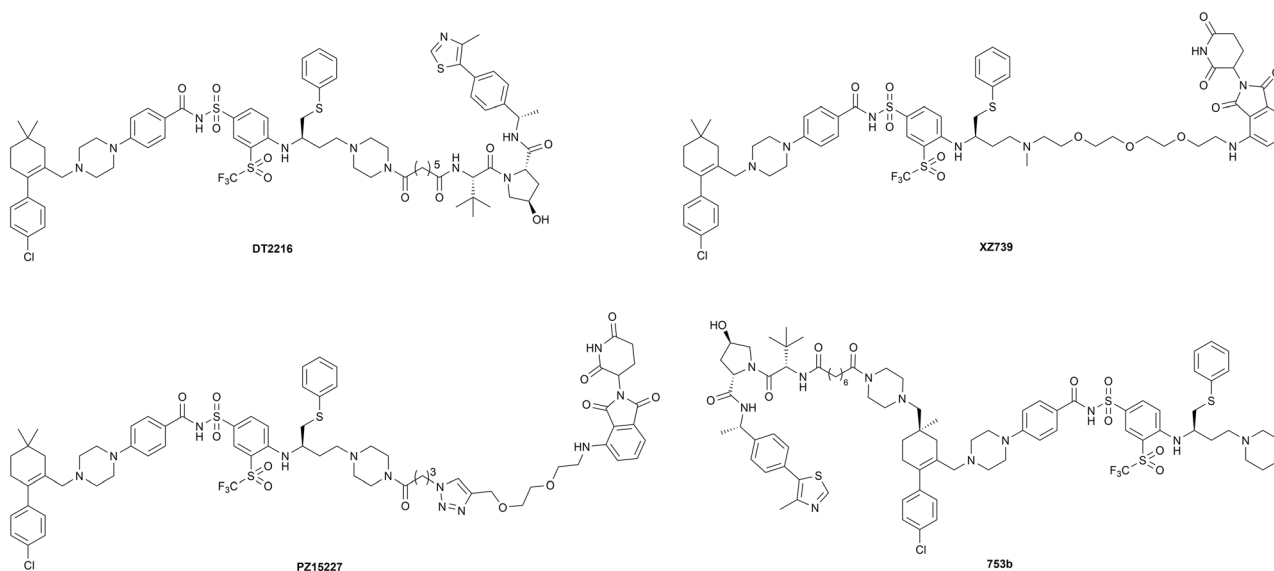


Fig. 2 Chemical structures of representative Bcl-xL/Bcl-2-targeting PROTACs.

cell/tissue selectivity with reduced on-target effects, even when targeting ubiquitously expressed proteins, as long as the E3 ligase has cell- or tissue-selective/specific expression.²⁹

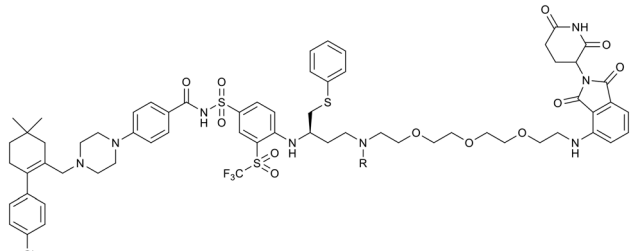
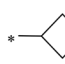
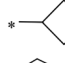
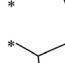
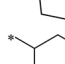
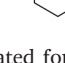
Our group has focused on developing Bcl-xL/Bcl-2 PROTAC degraders using various E3 ligases, including von Hippel-Lindau (VHL) and cereblon (CRBN) (Fig. 2).^{21–26} Among these, DT2216, a VHL-recruiting Bcl-xL selective degrader derived from ABT-263, demonstrated higher potency against a variety of Bcl-xL-dependent cancer cells with significantly reduced platelet toxicity compared to its parent compound ABT-263.²¹ DT2216 is currently in clinical trials (<https://ClinicalTrials.gov> IDs: NCT04886622 and NCT06620302). Building on this, we also developed XZ739, a CRBN-recruiting Bcl-xL degrader, by replacing the VHL-binding moiety in DT2216 with CRBN binding moiety pomalidomide, the piperazine group with an *N*-methylamine group, and the polymethylene linker with a PEG linker.²⁵ XZ739 exhibited over 7-fold higher potency than DT2216 against MOLT-4 cells (a T cell acute lymphoblastic leukemia (T-ALL) cell line that primarily depends on Bcl-xL for survival) and maintained excellent selectivity (>100-fold) for MOLT-4 cells over human platelets because CRBN E3 ligase and its associated E1 and E2 enzymes are minimally expressed in human platelets.²⁴ Similar to DT2216, no BCL-2 degradation was observed after treating with XZ739 in

MOLT-4 cells.²⁵ Our previous studies have revealed that both Bcl-xL and Bcl-2 can form stable ternary complexes with DT2216 and VHL in cell-free conditions, whereas in live cells, only Bcl-xL, but not Bcl-2, can form stable ternary complexes with DT2216 and VHL, which may contribute to the specificity of Bcl-xL degradation.²¹ These findings demonstrated the feasibility of achieving target specificity through conversion of non-selective inhibitors to PROTACs. However, whether the same mechanism exists for the selectivity of compound XZ739 on Bcl-xL needs to be validated by relevant experiments. In addition, while DT2216 displayed moderate cytotoxicity ($IC_{50} = 278$ nM) in NCI-H146 cells (a SCLC cell line that depends on both Bcl-xL and Bcl-2 for survival), XZ739 is more potent than DT2216 against NCI-H146 cells ($IC_{50} = 25$ nM), suggesting its potential as a single-agent treatment for tumors dependent on both Bcl-xL and Bcl-2 for survival. These findings laid a solid foundation for the further structural optimization of XZ739 as shown in this report.

Through a series of structure–activity relationship (SAR) studies, we identified PZ671 as a highly potent Bcl-xL degrader. PZ671 exhibited ~10-fold improved cellular activity against MOLT-4 cells ($IC_{50} = 1.3$ nM vs. 10.1 nM), ~6-fold enhanced degradation potency against Bcl-xL ($DC_{50} = 0.9$ nM vs. 5.1 nM) compared to XZ739 and demonstrated



Table 1 Bcl-xL degraders designed with various alkyl substituents at salt bridge nitrogen

Cmpd	R	IC ₅₀ ^a (nM)	K _i ^b	Cmpd	R	IC ₅₀ ^a (nM)	K _i ^b
ABT-263	—	202.3	0.26	1e		329.5	9.02
XZ739	CH ₃	10.1	0.31	1f		396.9	ND ^c
1a	H	59.7	0.27	1g		325.8	ND ^c
1b	CH ₂ CH ₃	52.8	0.38	1h		559.9	9.14
1c	CH(CH ₃) ₂	59.4	ND ^c	1i		>1000	ND ^c
1d		297.3	8.75				

^a IC₅₀ values are the means of at least three independent experiments; MOLT-4 cells were treated for 48 h. ^b Bcl-xL binding affinity; K_i values (in nM) are the means of at least three independent experiments. ^c ND: not determined.

superior potency across all tested SCLC cell lines. Importantly, PZ671 showed ~25-fold higher selectivity for MOLT-4 cells over platelets compared to ABT-263. *In vivo*, PZ671 effectively inhibited MOLT-4 xenograft tumor growth at a dosing regimen of 1.5 mg kg⁻¹ every 4 days but induced only a transient drop in platelet counts following its administration with rapid recovery observed from the second day onwards. This contrasts with the milder but more prolonged thrombocytopenic effects typically associated with VHL-recruiting degraders. We consider that the rapidly reversible platelet effects induced by the CRBN-recruiting degrader PZ671 may represent a more controllable therapeutic profile.

Results and discussion

Compound design and biological evaluation

As reported,^{23,30} Glu96 of Bcl-xL and the protonated nitrogen atom on the morpholine ring of ABT-263 form a salt bridge, which plays a crucial role in achieving high Bcl-xL binding affinity. Notably, the morpholine ring can be replaced with a dimethylamino group, as demonstrated in ABT-737. In our previous work, we designed XZ739 by replacing the morpholine ring in ABT-263 with an *N*-methylamino group as a linker attachment point. To investigate how different substituents at this position influence PROTAC activity, we systematically modified the substituents by either removing

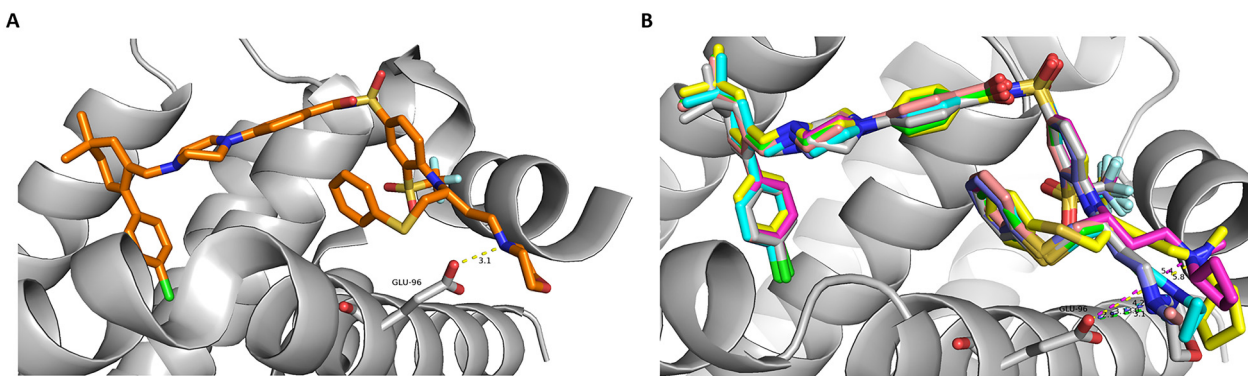


Fig. 3 Computational modelling of (A) ABT-263, available from PDB code 4QNQ and (B) derivatives with various alkyl substituents at the salt bridge nitrogen bound to Bcl-xL proteins. The bulky substituents push the nitrogen away from its optimal position to form a salt bridge with the Glu96 residue.



the methyl group or introducing various alkyl groups, yielding compounds **1a–1i** (Table 1).

These compounds were evaluated for their effects on the viability of MOLT-4 cells, with XZ739 as the positive control (Table 1 and Fig. S1A†). A clear trend was observed, larger substituents impaired cellular potency against MOLT-4 cells, with the effect becoming more pronounced as the substituent size increased. This is partly due to bulkier substituents disrupting the optimal positioning of the nitrogen atom for salt bridge formation, thereby decreasing Bcl-xL binding affinity (Table 1 and Fig. 3, S2 and S3†). However, other factors, such as the efficiency of forming stable ternary complexes, may also contribute. For example, compounds **1a/1b** exhibited similar binding affinity to XZ739 but were 5- to 6-fold less potent in killing MOLT-4 cells. Based on these findings, we retained the methyl-substituted tertiary amine in XZ739 and explored the impact of various linkages to the CRBN-recruiting moiety thalidomide/lenalidomide on cellular activity (Table 2 and Fig. S1B†).

Compound **2a**, featuring an ether linkage at the C4 position of thalidomide, exhibited comparable potency against MOLT-4 cells to XZ739. Replacing the ether linkage of **2a** with a triple bond **2b** resulted in a 2-fold increase in potency, while the corresponding saturated C–C linkage containing compound **2c** retained similar potency against MOLT-4 cells to **2b**. Moving the linker attachment to the C5 position of thalidomide significantly reduced potency for the triple-bond containing compound **3a** by almost 3-fold compared to the corresponding C4-substituted **2b**, whereas

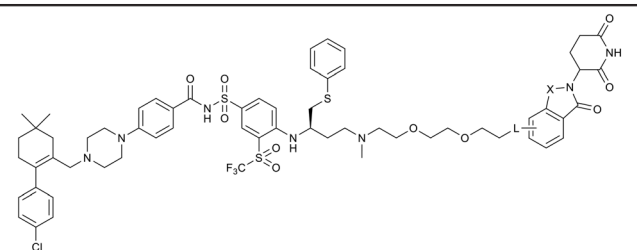
the C–C linkage compound **3b** showed cellular activity comparable to that of **2b/2c**.

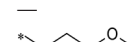
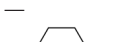

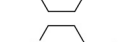
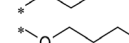
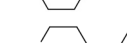

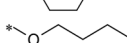

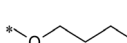
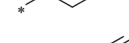
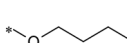
Incorporating conformationally restricted linkers has been shown to stabilize ternary complex formation and improve PK properties of PROTACs.^{31–35} To test this, we synthesized compounds **2d–2f** (Table 2) by inserting conformationally restricted units (piperazine/piperidine/triple bond) into the linker. Compound **2d** with a piperazine ring directly connected to thalidomide had similar cellular activity to XZ739 but was 2-fold weaker than **2b**. Introducing an additional triple bond between the piperidine ring and thalidomide (compound **2e**) reduced activity by ~4-fold compared to **2d**. Reducing the triple bond in **2e** to a saturated ethylene (compound **2f**) resulted in slightly lower potency in MOLT-4 cells than **2e**. These results suggest that introducing ring systems, whether at the linker terminus or in the middle, negatively impact activity.

Lenalidomide often offers advantages over thalidomide as a CRBN-recruiting ligand due to its improved metabolic and chemical stability, attributed to the absence of a phthalimide carbonyl group.^{36,37} Incorporating lenalidomide with the effective C–C linkage at the C4 or C5 positions, we synthesize compounds **4a**, **4b** and **5b**. The cellular activity of these compounds was significantly improved, with the C5-substituted ethylene linkage compound **5b** (PZ671, Fig. 4A) showing an 8-fold increase in potency against MOLT-4 cells compared to XZ739.

PZ671 was selected for further evaluation. We evaluated PZ671 in comparison to XZ739 for their cell killing effects on

Table 2 Bcl-xL degraders designed with various linkages and substituted positions to thalidomide/lenalidomide



X	Substitution position	Cmpd	L	IC ₅₀ ^a (nM)	Cmpd	L	IC ₅₀ ^a (nM)
		ABT-263	—	202.3	XZ739	—	10.1
CO	C4-	2a		10.4	2d		10.6
		2b		5.2	2e		36.1
		2c		6.2	2f		45.5
	C5-	3a		14.3	3b		4.3
CH ₂	C4-	4a		4.1	4b		4.5
	C5-	5a		2.1	5b (PZ671)		1.3

^a IC₅₀ values are the means of at least three independent experiments; MOLT-4 cells were treated for 48 h.



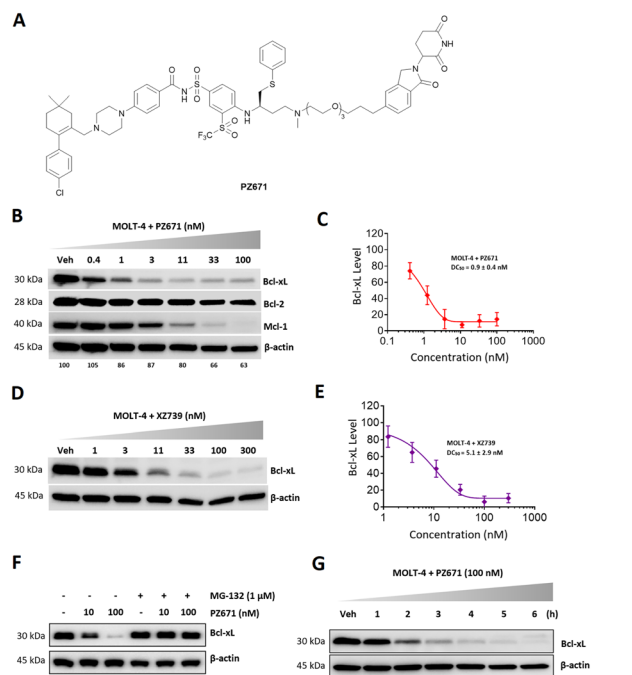


Fig. 4 PZ671-induced Bcl-xL degradation. (A) The structure of PZ671. (B and D) Representative western blotting analysis of protein levels in MOLT-4 cells after treatment with indicated concentrations of PZ671 and XZ739 for 16 h. Percentage decrease in β -actin levels due to toxicity was normalized to the control sample. Data representative of 3 independent experiments. (C and E) Densitometric analysis of Bcl-xL expression in MOLT-4 cells. The data presented are mean \pm SD of three independent experiments. (F) Pretreatment with 1 μ M MG-132 for 2 h blocked the degradation of Bcl-xL induced by PZ671. (G) Bcl-xL levels in MOLT-4 cells treated with 100 nM PZ671 at the indicated time points.

a panel of SCLC cell lines (Fig. S4[†]). The results revealed that PZ671 is more potent than XZ739 against all tested SCLC cell lines. Western blot analysis confirmed that PZ671 induced dose-dependent Bcl-xL degradation in MOLT-4 cells (Fig. 4B and S5A[†]) and had a better degradation potency against Bcl-xL than XZ739, with a DC_{50} value of 0.9 nM (Fig. 4C) compared to a DC_{50} value of 5.1 nM for XZ739 (Fig. 4D and E). This degradation was blocked by proteasome inhibitor MG-132 (Fig. 4F and S5C[†]), indicating a proteasome-dependent mechanism. Furthermore, the Bcl-xL degradation induced by PZ671 in MOLT-4 cells was rapid, with Bcl-xL protein levels significantly reduced within 2 h of treatment, and almost complete degradation observed 4 h after exposure to 100 nM PZ671 (Fig. 4G and S5D and E[†]).

We next assessed the impact of PZ671 on apoptosis. Western blot analysis showed that PZ671 dose-dependently increased poly(ADP-ribose) polymerase (PARP) and caspase-3 cleavage in MOLT-4 cells (Fig. 5A and S6[†]), suggesting the apoptotic cell-death mechanism. Notably, we observed a significant reduction in β -actin levels with increasing concentrations of PZ671 in this experiment. MOLT4 T-ALL cells are highly sensitive to Bcl-xL degradation and can rapidly undergo apoptosis upon Bcl-xL loss. In line with our

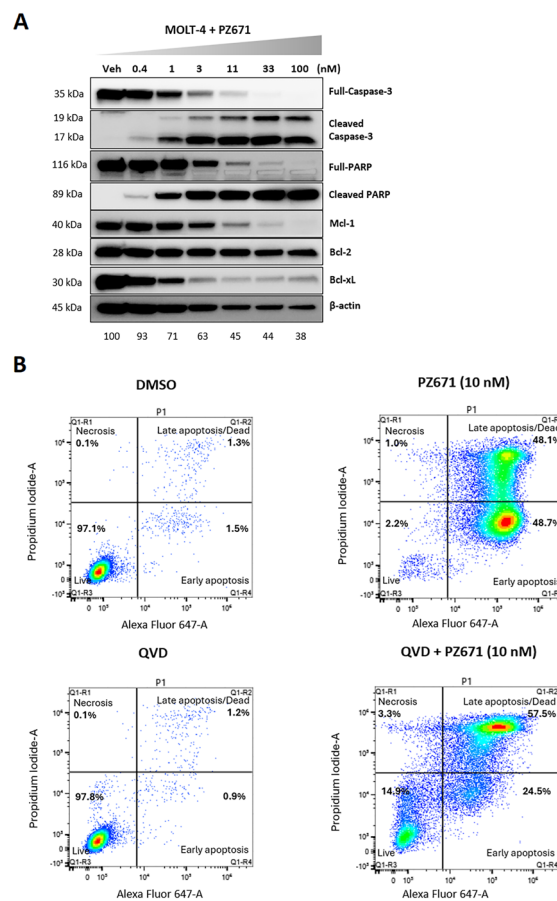


Fig. 5 Characterization of PZ671-mediated apoptosis in MOLT-4 cells. (A) Western blot analysis of cleaved PARP and cleaved caspase-3 after 16 h of treatment with indicated concentrations of PZ671. The full-PARP blot was from the stripped membrane and re-probed with cleaved PARP, resulting in the rectangular shape. Percentage decrease in β -actin levels due to toxicity was normalized to the control sample. (B) Flow cytometry analysis of apoptosis using annexin V and PI staining. MOLT-4 cells were treated with PZ671 at 10 nM for 24 h. PZ671 significantly increased the percentage of apoptotic cells and QVD (10 μ M) pretreatment for 2 h inhibited the apoptosis induced by PZ671. Data are representative of two independent experiments.

previous observation that 100 nM PZ671 nearly completely degrades Bcl-xL within 4 h (Fig. 4G), we hypothesize that PZ671-induced cell death at higher concentrations may partially account for the observed β -actin decrease. However, since this effect was not consistently observed across all cases, additional factors influencing β -actin levels may be involved and warrant further investigation. The apoptotic cell-death mechanism is further supported by flow cytometry analysis of annexin V and propidium iodide (PI) staining (Fig. 5B), which showed that PZ671-induced apoptosis was attenuated by pretreatment of MOLT-4 cells with the pan-caspase inhibitor Q-VD-Oph (QVD).

In human platelets, PZ671 degraded Bcl-xL at concentrations above 1 μ M (Fig. 6A and S7[†]), whereas XZ739 showed no degradation at the same concentrations.²⁵ Consistent with the degradation result, the selectivity of PZ671 for MOLT-4 cells over platelets was reduced compared



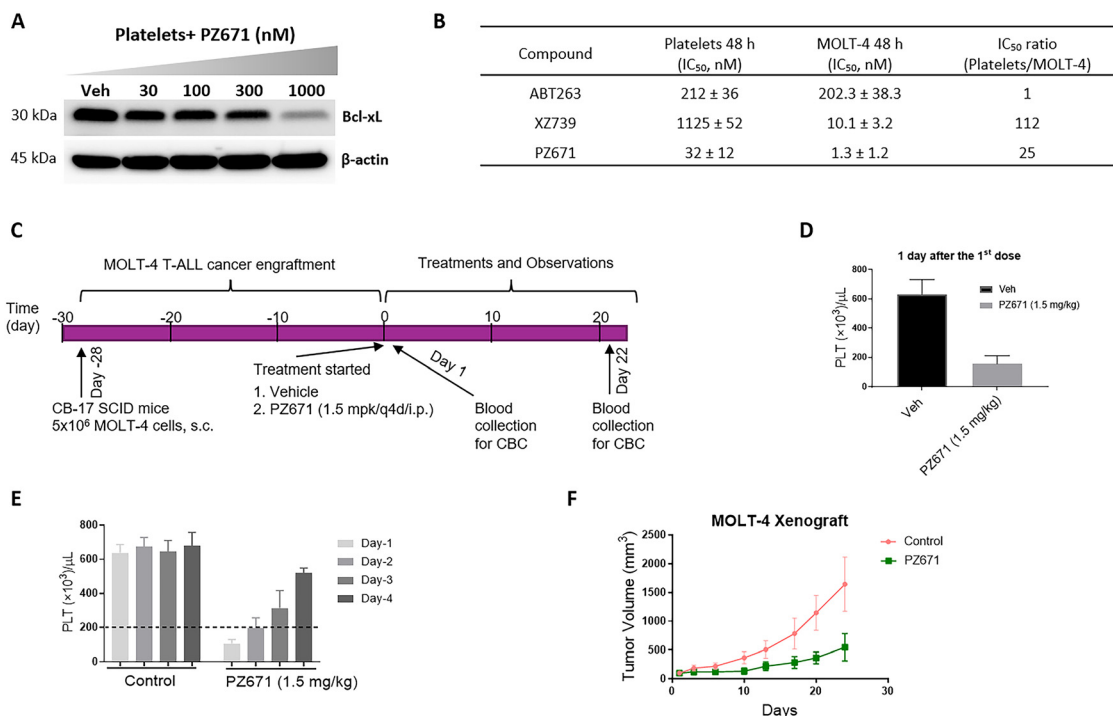


Fig. 6 (A) Western blot showing the Bcl-xL levels in human platelets treated with the indicated concentration of PZ671 for 48 h. (B) A comparison of cellular activity of selected compounds in human platelets and MOLT-4 cells. (C) Illustration of the experiment design of MOLT-4 T-ALL cancer xenograft model. (D) Blood platelet (PLT) counts in mice were measured 1 day after receiving the first dose of vehicle (Veh) or PZ671. The data presented are mean \pm SD ($n = 3$ mice per group). (E) Changes in blood platelet (PLT) counts in mice were measured during one cycle after administration of vehicle (control) and PZ671. The data presented are mean \pm SD ($n = 3$ mice per group). (F) Changes in tumor volume over time after the start of treatment.

to XZ739 (25-fold vs. 137-fold) (Fig. 6B and S8[†]). *In vivo*, PZ671 caused a transient \sim 72% reduction in platelet counts after a single dose (1.5 mg kg⁻¹, i.p.) in MOLT-4 xenograft mice, with rapid recovery observed from the second day onward (Fig. 6C–E). Clinically, we believe the transient platelet reduction could be more manageable with optimized dosing regimen. Importantly, there is clear evidence that PZ671 treatment (1.5 mg kg⁻¹, Q4D, i.p.) markedly suppressed the tumor growth (Fig. 6F).

Chemistry

The synthesis of PROTAC **1a** is outlined in Scheme 1. Briefly, SNAr substitution of 4-fluorothalidomide **6** with azide **7** under microwave irradiation afforded compound **8**. Palladium-catalyzed hydrogenation of **8** resulted in compound **9**. Coupling of precursor acid **10** with sulfonamide **11** in the presence of EDCI and DMAP afforded compound **12**, which was reduced to aldehyde by treating with DIBAL-H to give compound **13**. Aldehyde **13** was subjected to reductive amination with **9** to generate the final product **1a**. Compounds **7**,³⁸ **10**,³⁹ and **11**⁴⁰ were prepared as reported.

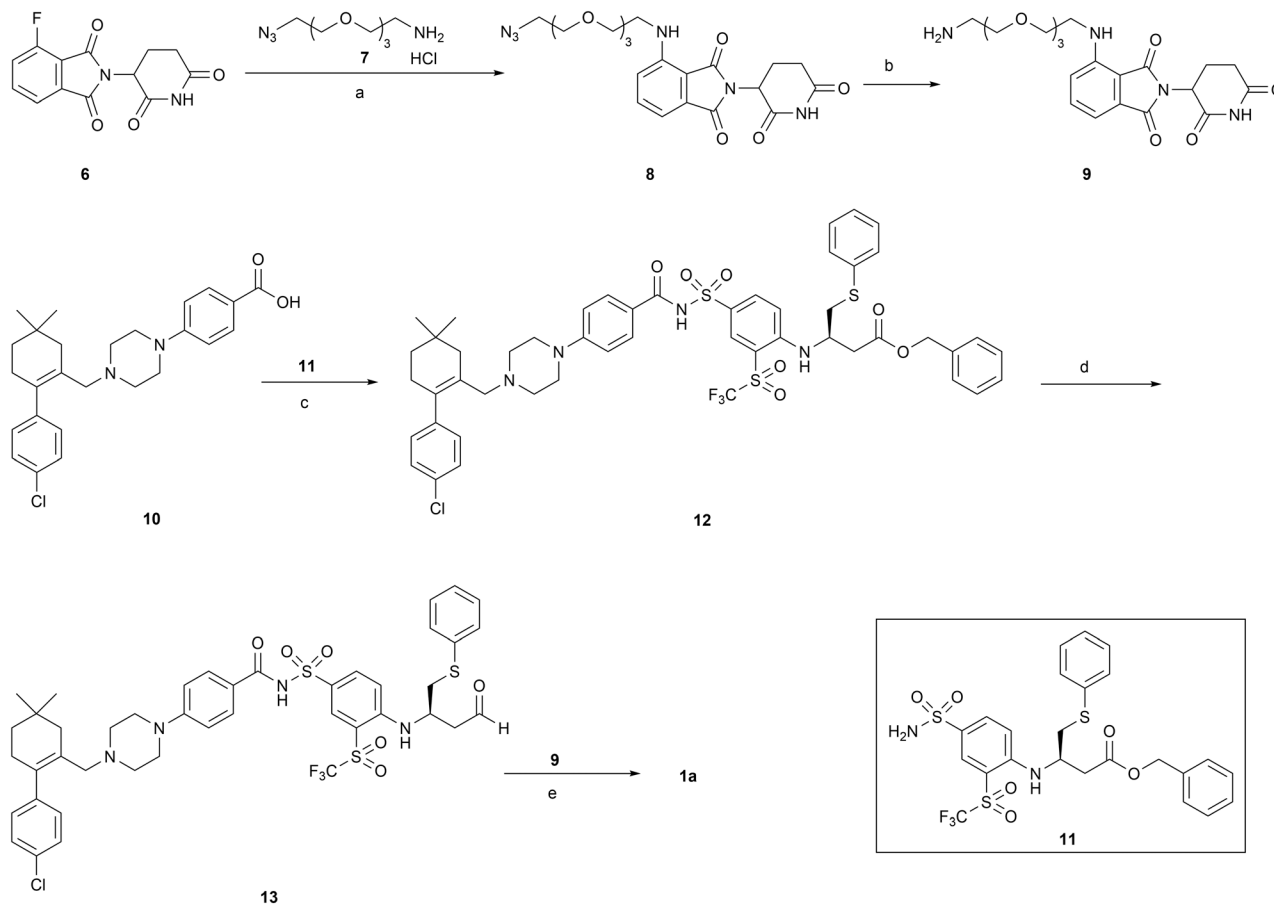
Pomalidomide-based PROTACs **1b**, **1c**, and **1e–1i** with various substitutions on the salt bridge nitrogen were synthesized by reductive amination of **1a** with the

corresponding aldehyde (**14a** and **14b**) or ketone (**15a–15e**) (Scheme 2). Compound **1d** was produced through nucleophilic substitution of **1a** with bromocyclopropane **16**.

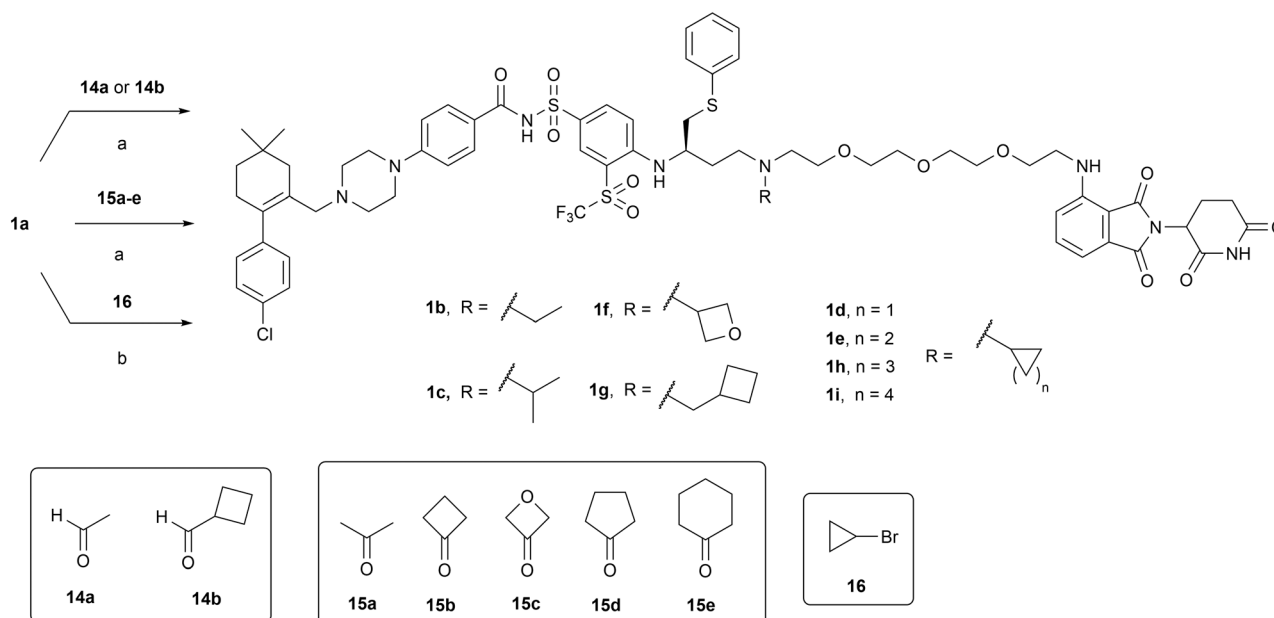
The syntheses of PROTACs **2a–2d**, **3a**, **3b**, **4a**, **4b**, **5a**, and **5b** are outlined in Schemes 3–6. Tosylate PEG linker precursor **20** was synthesized as previously reported.⁴¹ It was then reacted with 4-OH-thalidomide **21** in the presence of NaHCO₃ and KI at 80 °C to yield compound **22**. Removal of the Boc group of **22**, followed by reductive amination with aldehyde **13**, yielded the final product **2a** (Scheme 3). Terminal alkyne linker precursor **25** was prepared by tosylation of the OH group of starting material **23**, followed by treating with a methylamine ethanol solution (33 wt%) and Boc protection. Sonogashira coupling of **25** with 4- or 5-bromo-substituted thalidomide/lenalidomide derivatives **26a–26d** afforded intermediates **27a–27d**, which were subsequently reduced to the corresponding saturated C–C linkage compounds **28a–28d** under palladium-catalyzed hydrogenation. Final products **2b**, **2c**, **3a**, **3b**, **4a**, **4b**, **5a**, and **5b** (PZ671) were synthesized *via* reductive amination of the corresponding de-Boc intermediates with aldehyde **13** (Scheme 4).

The synthesis of compound **2d** is shown in Scheme 5. Key intermediate **32** was obtained *via* SNAr substitution of **6** with Boc-protected piperazine **30**, followed by Boc deprotection





Scheme 1 Reagents and conditions: (a) DIPEA, DMSO, MW, 100 °C; (b) Pd/C, H₂, MeOH, rt; (c) EDCI, DMAP, DCM, rt; (d) DIBAL-H, toluene, -78 °C; (e) NaBH(OAc)₃, DCM, rt.

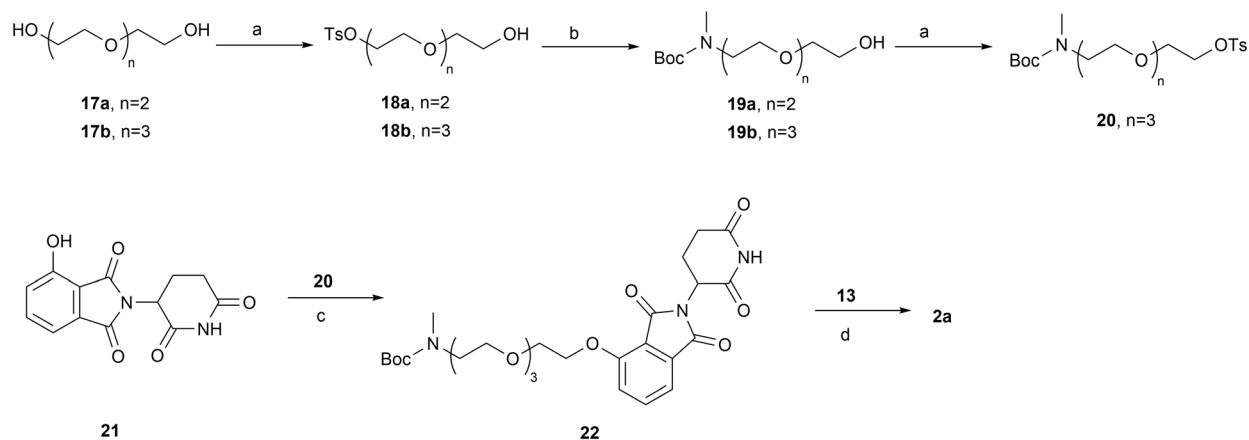


Scheme 2 Reagents and conditions: (a) NaBH(OAc)₃, DCE, 50 °C; (b) DIPEA, EtOH, 65 °C.

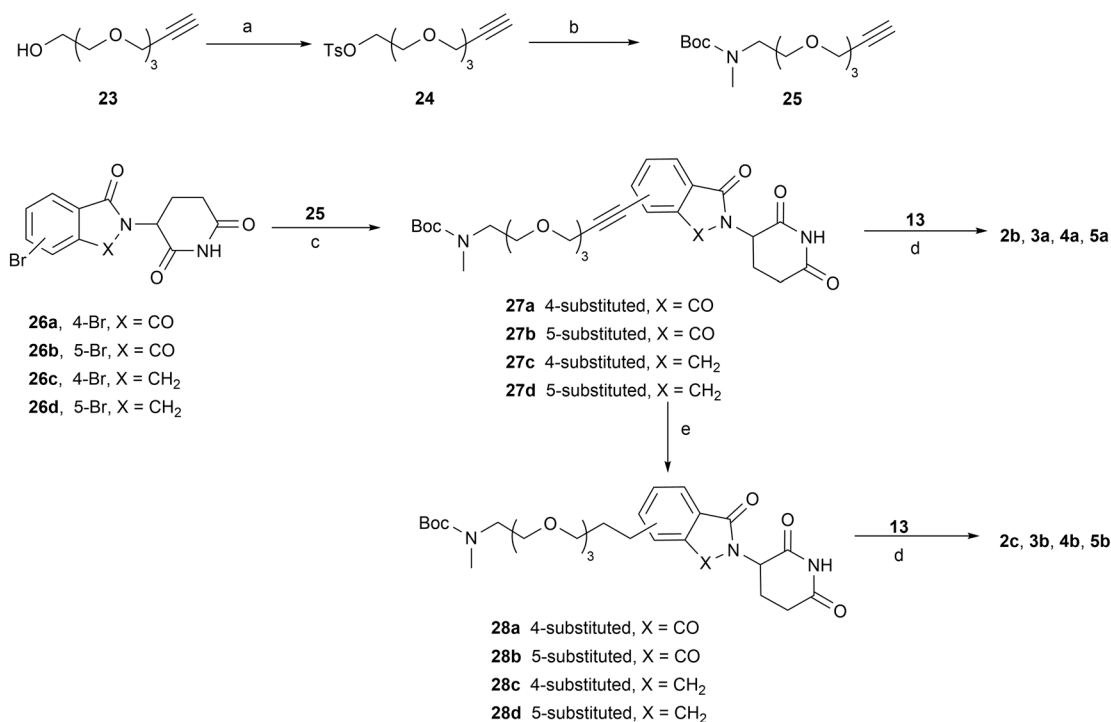
and reductive amination with compound **29**. Compound **29** was produced by treating **19a** with Dess–Martin periodinane.

Subsequent Boc deprotection of **32** and reductive amination with aldehyde **13** gave the final product **2d**. Compound **2e**





Scheme 3 Reagents and conditions: (a) TsCl, TEA, DCM, rt; (b) (i) MeNH₂, EtOH, 70 °C; (ii) Boc₂O, TEA, DCM, rt; (c) NaHCO₃, KI, DMF, 80 °C; (d) (i) HCl/1,4-dioxane, DCM, rt; (ii) NaBH(OAc)₃, DCM, rt.



Scheme 4 Reagents and conditions: (a) TsCl, TEA, DCM, rt; (b) (i) MeNH₂, EtOH, 90 °C; (ii) Boc₂O, TEA, DCM, rt; (c) PdCl₂(PPh₃)₂, PPh₃, CuI, TEA, DMF, 90 °C; (d) (i) HCl/1,4-dioxane, DCM, rt; (ii) NaBH(OAc)₃, DCM, rt; (e) Pd/C, H₂, MeOH, rt.

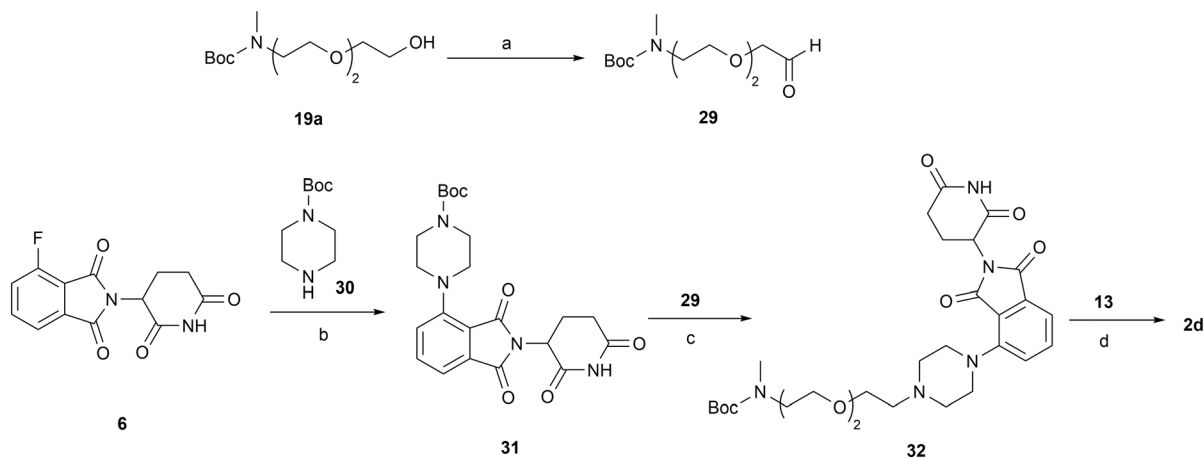
was prepared *via* Sonogashira coupling of **26a** with **33**, followed by Boc deprotection group and reductive amination with **29** to afford compound **35**, then a second round of de-Boc and reductive amination with aldehyde **13**. Similarly, compound **2f** was synthesized from the triple bond-saturated intermediate **36** (Scheme 6).

Conclusions

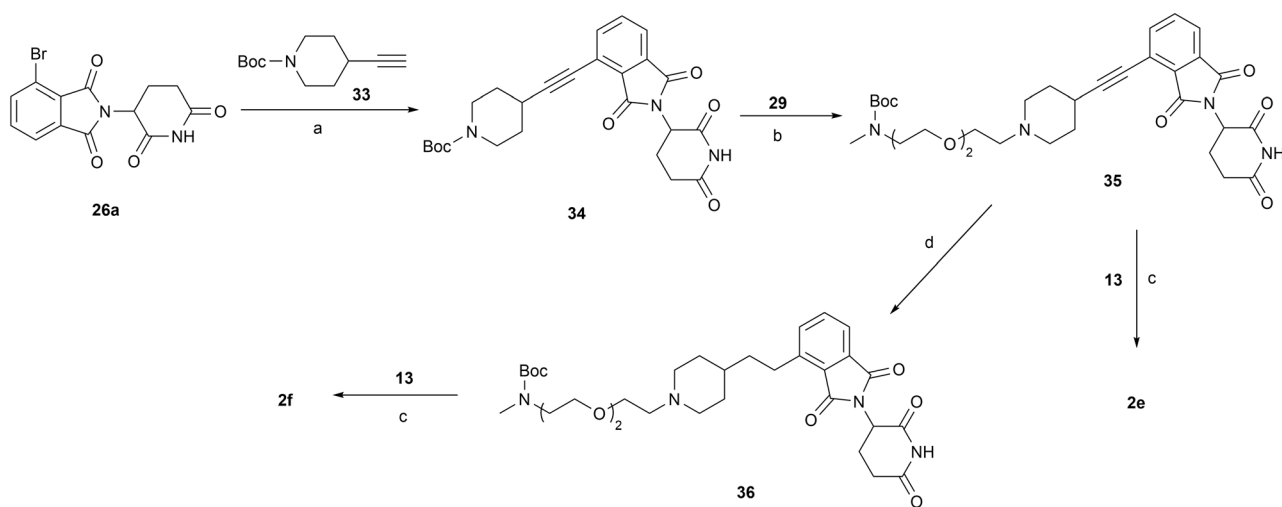
In this study, based on the lead compound XZ739, we systematically investigated the effects of substituent size on the salt-bridge nitrogen, a crucial interaction for high Bcl-xL

binding, and explored alternative CRBN-recruiting moieties connected *via* various linkages. We identified PZ671, which utilizes lenalidomide as the CRBN-recruiting moiety with an ethylene linkage at the C5-position of the benzene ring of lenalidomide. PZ671 exhibited ~10-fold higher potency against MOLT-4 cells and ~6-fold enhanced degradation efficacy against target Bcl-xL compared to XZ739, although its selectivity for MOLT-4 cells over platelets decreased ~5-fold (112-fold *vs.* 25-fold). Despite this trade-off, the enhanced cellular activity may translate into a broader anticancer spectrum. *In vivo* studies revealed that unlike the mild but sustained platelet toxicity caused by VHL-recruiting Bcl-xL/





Scheme 5 Reagents and conditions: (a) Dess–Martin periodinane, DCM, rt; (b) DIPEA, DMSO, MW, 90 °C; (c) (i) HCl/1,4-dioxane, DCM, rt; (ii) NaBH(OAc)₃, DCM, rt; (d) (i) HCl/1,4-dioxane, DCM, rt; (ii) NaBH(OAc)₃, DCM, rt.



Scheme 6 Reagents and conditions: (a) PdCl₂(PPh₃)₂, CuI, TEA, DMSO, 90 °C; (b) (i) HCl/1,4-dioxane, DCM, rt; (ii) NaBH(OAc)₃, DCM, rt; (c) (i) HCl/1,4-dioxane, DCM, rt; (ii) NaBH(OAc)₃, DCM, rt; (d) Pd/C, H₂, MeOH, rt.

Bcl-2 degrader 753b, the platelet toxicity of CRBN-recruiting degrader PZ671 was more prominent but transient, with maximal effect on the first day post-administration followed by rapid recovery. This transient toxicity profile may be more manageable clinically with appropriately optimized dosing regimens. Further efforts will focus on conjugating novel CRBN-recruiting ligands and exploring alternative linker attachment positions, such as utilizing the P2 pocket of ABT-263, which has proven effective in modifying VHL-recruiting Bcl-xL/Bcl-2 degraders to enhance cellular activity and degradation.

Experimental section

Chemistry

The synthetic procedures along with the characterization data of all compounds are reported in the ESI.†

Biological assays

AlphaScreen binary binding assay. Assays were performed at room temperature. All reagents were diluted in a buffer containing 25 mM HEPES, pH 7.5, 100 mM NaCl, 0.1% BSA, and 0.015% Tween 80. To a 96-well PCR plate (Thermo Scientific, Cat. No. AB-1400) were added His-tagged Bcl-xL protein (10 μL, 4 nM, Cat. No. SRP0187, Sigma-Aldrich), testing compound (10 μL, 3-fold serial dilution) and biotin-tagged BAD (10 μL, 10 nM, biotin-LWAAQRYGRELRRMSDEFEGSFKGL amino-terminal, AnaSpec). The mixed solution was incubated at room temperature for 1 h, anti-6×His acceptor beads (5 μL, 160 μg mL⁻¹, PerkinElmer, Cat. No. AL128M) were added to each well under subdued light, then incubated for an additional 20 min in the dark. Streptavidin-donor beads (5 μL, 160 μg mL⁻¹, Cat. No. 6760002, PerkinElmer) were added to each well under subdued light, then incubated for an additional 30 min in the dark. The resulting solution in each



well was transferred to two adjacent wells (17 μL each) of a 384-well white OptiPlate (PerkinElmer, Cat. No. 6008280). The 384-well plate was scanned on a Biotek Synergy Neo2 multi-mode plate reader installed with an AlphaScreen filter cube. The K_i values of each compound were calculated by using the “binding-competitive, one site-Fit K_i ” function in GraphPad Prism 10 based on concentrations of biotin-peptide used and experimentally determined K_d values of each 6 \times His protein and biotin-peptide pair.

Cell lines and culture

MOLT-4 T-ALL (Cat# CRL-1582) cell line was purchased from American Type Culture Collection (ATCC, Manassas, VA). MOLT-4 cells were cultured in RPMI 1640 medium (Life Technologies, Carlsbad, CA, USA) supplemented with 10% FBS (Atlanta Biologicals, Flowery Branch, GA, USA) and 1% penicillin–streptomycin solution (Thermo Fisher Scientific, Waltham, MA, USA). The SCLC cell lines, except H146, were obtained from the NCI-Navy Medical Oncology source supply as stated in our previous publication.⁴² H146 cells were obtained from ATCC. The cell lines were cultured as reported previously.⁴² The stocks of the cell lines were STR profiled by the NIH or ATCC. All cultures were tested for mycoplasma negativity using the MycoAlert Mycoplasma Detection Kit (Cat. No. LT07–318, Lonza, Basel, Switzerland). The cell lines were maintained in a humidified incubator at 37 $^\circ\text{C}$ and 5% CO_2 .

Cell viability assay

Cell viability was measured by tetrazolium-based MTS assay (Promega, Madison, WI, USA). 5×10^4 to 1×10^5 suspension cells were seeded and treated in 96-well plates for 48 h or 72 h. The IC_{50} values of individual agents were calculated with GraphPad Prism 7 software (GraphPad Software, La Jolla, CA, USA).

Immunoblotting

Cells were collected and lysed in lysis buffer (Boston Bio Products, Ashland, MA, USA) supplemented with protease and phosphatase inhibitor cocktails (Sigma-Aldrich, St. Louis, MO, USA). An equal amount of protein lysates was separated on pre-casted 4–20% Tris-glycine gels (Bio-Rad, Hercules, CA, USA). Thereafter, the proteins were transferred to PVDF membranes (MilliporeSigma, Billerica, MA, USA). The membranes were blocked with 5% (w/v) non-fat dry milk in TBS + Tween 20 (0.1% (v/v)), and then probed with primary antibodies overnight at 4 $^\circ\text{C}$. Next day, the membranes were washed and incubated with appropriate HRP-conjugated secondary antibodies. The signal was detected using ECL substrate (MilliporeSigma) and captured on X-ray films or ChemiDoc MP Imaging System (Bio-Rad). The band intensities were calculated on ImageJ software and normalized to equal loading control β -actin.

Human platelet isolation and viability assays

Platelet-rich plasma (PRP) was purchased from Life South Community Blood Center (Gainesville, FL, USA). PRP was transferred into a 50 mL tube containing 5 mL acid citrate buffer (Cat. No. sc-214744, Santa Cruz Biotechnology). To prevent clotting, prostaglandin E1 (PGE1, Cat. No. sc-201223A, Santa Cruz Biotechnology) and apyrase (Cat. No. A6237, Sigma-Aldrich) were added to final concentrations of 1 μM and 0.2 units per mL, respectively. After gently mixing the solution, platelets were pelleted by centrifugation at 1200g for 10 min without break. Pelleted platelets were gently washed without disrupting the platelets in 2 mL HEPES Tyrode's buffer (Cat. No. PY-921WB, Boston BioProducts, Ashland, MA, USA) containing 1 μM PGE1 and 0.2 units per mL apyrase. After washing, pellets were slowly suspended in 10 mL HEPES Tyrode's buffer containing 1 μM PGE1 and 0.2 units per mL apyrase. Then platelets number was counted using a HEMAVET 950FS hematology analyzer (Drew Scientific, Inc., Oxford, CT, USA). For viability assays, platelet number was adjusted to 2×10^8 per mL in HEPES Tyrode's buffer containing 1 μM PGE1 and 0.2 units per mL apyrase. Each treatment was given in 2 mL platelet suspensions in 15 mL polypropylene tubes. The tubes were placed on a rotating platform at room temperature and the viability of platelets was measured after 24 h of treatment by using MTS reagent (Cat. No. G1111, Promega, Madison, WI, USA). The data were analyzed using GraphPad Prism 7 software for the calculation of IC_{50} values.

Flow cytometry

MOLT-4 cells were seeded in 12-well plates at a density of 4×10^5 cells per well and pretreated with or without Q-VD-Oph (QVD, Cat. No. S7311, Selleckchem, Houston, TX, USA) for 4 h. After pretreatment, cells were treated with PZ671 (10 nM) for 48 h. Caspase activity was blocked using QVD pretreatment for 2 h. After treatment, cells were stained with Alexa Fluor 647-annexin V (1:50, Cat. No. 640912, BioLegend, San Diego, CA, USA) and PI (10 $\mu\text{g mL}^{-1}$, Cat. No. 421301, BioLegend, San Diego, CA, USA) at room temperature for 30 min. For apoptosis analysis, the stained cells were analyzed on an Aurora flow cytometer (Cytex Aurora, Fremont, CA, USA).

MOLT-4 T-ALL xenograft mouse model

To test the effect of PZ671 on tumor growth in MOLT-4 T-ALL xenografts, MOLT-4 T-ALL cells were collected and suspended in regular RPMI medium and mixed with Matrigel (1:1) (cat. no. 356231, Corning). The cells (5×10^6 cells) suspended in 100 μL of RPMI medium–Matrigel mixture were subcutaneously (s.c.) implanted in the right flank of 5 week-old CB-17 SCID mice purchased from the Charles River Laboratories (Wilmington, MA, USA). Tumor growth was monitored daily, and tumors were measured twice per week using a vernier caliper or digital calipers. Tumor volume was determined using the formula $(L \times W^2) \times 0.5$, where L is the



length in mm and W is the width in mm. The treatment started once the average tumor volume reached $\sim 150 \text{ mm}^3$. The animals were randomly assigned into separate groups ($n = 6$ animals per group) such that each group had nearly equal starting average tumor volume and started undergoing treatment with vehicle (i.p., 100 μL per injection) and PZ671 (1.5 mg kg^{-1} , every 4 days, i.p., 100 μL per injection). PZ671 for i.p. administration was formulated in 50% Phosal 50 PG, 45% Miglyol 810 N and 5% polysorbate 80.

In vivo platelet toxicity assays

Female 5–6 weeks old CB-17 SCID-beige mice were treated with single i.p. doses of PZ671 (1.5 mg per kg body weight). Approximately 50 μL blood was collected every day for 4 days *via* submandibular plexus route in EDTA tubes (RAM Scientific), and platelets were enumerated using an automated hematology analyzer (HEMAVET 950FS, Drew Scientific Inc., Miami Lakes, FL, USA).

Ethical statement

All animal procedures were performed in accordance with the guidelines of the Institutional Animal Care and Use Committee (IACUC) of the University of Florida and approved by the animal ethics committee of the University of Florida under protocol # 201710069.

Data availability

ESI† to this article can be found online. Additional data will be made available upon request as reasonably possible.

Conflicts of interest

The authors declare the following competing financial interest(s): P. Zhang, S. Khan, X. Zhang, D. Zhou, and G. Zheng are co-inventors for Bcl-xL PROTACs disclosed in this study. D. Zhou and G. Zheng are co-founders and shareholders of Dialectic Therapeutics, a company that is developing Bcl-xL PROTACs to treat cancers.

Acknowledgements

This study was supported in part by NIH grants R01CA241191 and R01CA260239.

Notes and references

- S. Elmore, *Toxicol. Pathol.*, 2007, **35**, 495–516.
- D. Hanahan and R. A. Weinberg, *Cell*, 2011, **144**, 646–674.
- J. M. Adams and S. Cory, *Oncogene*, 2007, **26**, 1324–1337.
- R. J. Youle and A. Strasser, *Nat. Rev. Mol. Cell Biol.*, 2008, **9**, 47–59.
- J. K. Brunelle and A. Letai, *J. Cell Sci.*, 2009, **122**, 437–441.
- P. E. Czabotar, G. Lessene, A. Strasser and J. M. Adams, *Nat. Rev. Mol. Cell Biol.*, 2014, **15**, 49–63.
- P. D. Bhola and A. Letai, *Mol. Cell*, 2016, **61**, 695–704.
- M. Vogler, *Adv. Med.*, 2014, **2014**, 943648.
- S. A. Amundson, T. G. Myers, D. Scudiero, S. Kitada, J. C. Reed and A. J. Fornace, *Cancer Res.*, 2000, **60**, 6101–6110.
- J. Chang, Y. Wang, L. Shao, R. M. Laberge, M. Demaria, J. Campisi, K. Janakiraman, N. E. Sharpless, S. Ding, W. Feng, Y. Luo, X. Wang, N. Aykin-Burns, K. Krager, U. Ponnappan, M. Hauer-Jensen, A. Meng and D. Zhou, *Nat. Med.*, 2016, **22**, 78–83.
- R. Yosef, N. Pilpel, R. Tokarsky-Amiel, A. Biran, Y. Ovadya, S. Cohen, E. Vadai, L. Dassa, E. Shahar, R. Condiotti, I. Ben-Porath and V. Krizhanovsky, *Nat. Commun.*, 2016, **7**, 11190.
- Y. Zhu, T. Tchkonja, H. Fuhrmann-Stroissnigg, H. M. Dai, Y. Y. Ling, M. B. Stout, T. Pirtskhalava, N. Giorgadze, K. O. Johnson, C. B. Giles, J. D. Wren, L. J. Niedernhofer, P. D. Robbins and J. L. Kirkland, *Aging Cell*, 2016, **15**, 428–435.
- P. Pal, P. Zhang, S. Poddar and G. Zheng, *Expert Opin. Ther. Pat.*, 2022, **32**, 1003–1026.
- T. Oltersdorf, S. W. Elmore, A. R. Shoemaker, R. C. Armstrong, D. J. Augeri, B. A. Belli, M. Bruncko, T. L. Deckwerth, J. Dinges, P. J. Hajduk, M. K. Joseph, S. Kitada, S. J. Korsmeyer, A. R. Kunzer, A. Letai, C. Li, M. J. Mitten, D. G. Nettesheim, S. Ng, P. M. Nimmer, J. M. O'Connor, A. Oleksijew, A. M. Petros, J. C. Reed, W. Shen, S. K. Tahir, C. B. Thompson, K. J. Tomaselli, B. Wang, M. D. Wendt, H. Zhang, S. W. Fesik and S. H. Rosenberg, *Nature*, 2005, **435**, 677–681.
- M. Bruncko, T. K. Oost, B. A. Belli, H. Ding, M. K. Joseph, A. Kunzer, D. Martineau, W. J. McClellan, M. Mitten, S. Ng, P. M. Nimmer, T. Oltersdorf, C. Park, A. M. Petros, A. R. Shoemaker, X. Song, X. Wang, M. D. Wendt, H. Zhang, S. W. Fesik, S. H. Rosenberg and S. W. Elmore, *J. Med. Chem.*, 2007, **50**, 641–662.
- C. Tse, A. R. Shoemaker, J. Adickes, M. G. Anderson, J. Chen, S. Jin, E. F. Johnson, K. C. Marsh, M. J. Mitten, P. Nimmer, L. Roberts, S. K. Tahir, Y. Xiao, X. Yang, H. Zhang, S. Fesik, S. H. Rosenberg and S. W. Elmore, *Cancer Res.*, 2008, **68**, 3421–3428.
- L. Bai, J. Chen, L. Liu, D. McEachern, A. Aguilar, H. Zhou, C. Y. Yang, H. Wang, J. Wen, G. Wang, Y. Zhai, M. Guo, D. Yang and S. Wang, *Eur. J. Cancer.*, 2014, **50**, 109–110.
- A. W. Tolcher, B. A. Carneiro, A. Dowlati, A. R. A. Razak, Y. K. Chae, J. A. Villella, S. Coppola, S. Englert, A. C. Phillips, A. J. Souers, Z. Salman, S. Penugonda, J. D. Powderly and P. LoRusso, *J. Clin. Oncol.*, 2021, **39**, 3015.
- X. Zhang, D. Thummuri, Y. He, X. Liu, P. Zhang, D. Zhou and G. Zheng, *Chem. Commun.*, 2019, **55**, 14765–14768.
- X. Zhang, Y. He, P. Zhang, V. Budamagunta, D. Lv, D. D. Thummuri, Y. Yang, J. Pei, Y. Yuan, D. Zhou and G. Zheng, *Eur. J. Med. Chem.*, 2020, **199**, 112397.
- S. Khan, X. Zhang, D. Lv, Q. Zhang, Y. He, P. Zhang, X. Liu, D. Thummuri, Y. Yuan, J. S. Wiegand, J. Pei, W. Zhang, A. Sharma, C. R. McCurdy, V. M. Kuruvilla, N. Baran, A. A. Ferrando, Y. Kim, A. Rogojina, P. J. Houghton, G. Huang, R. Hromas, M. Konopleva, G. Zheng and D. Zhou, *Nat. Med.*, 2019, **25**, 1938–1947.



- 22 D. Lv, P. Pal, X. Liu, Y. Jia, D. Thummuri, P. Zhang, W. Hu, J. Pei, Q. Zhang, S. Zhou, S. Khan, X. Zhang, N. Hua, Q. Yang, S. Arango, W. Zhang, D. Nayak, S. K. Olsen, S. T. Weintraub, R. Hromas, M. Konopleva, Y. Yuan, G. Zheng and D. Zhou, *Nat. Commun.*, 2021, **12**, 6896.
- 23 D. Nayak, Y. Lv, P. Yuan, W. Zhang, A. Hu, E. A. Nayak, Z. Ruben, P. Lv, R. Sung, G. Hromas, D. Zhou Zheng and S. K. Olsen, *Nat. Commun.*, 2024, **15**, 2743.
- 24 Y. He, X. Zhang, J. Chang, H. Kim, P. Zhang, Y. Wang, S. Khan, X. Liu, X. Zhang, D. Lv, L. Song, W. Li, D. Thummuri, Y. Yuan, J. S. Wiegand, Y. T. Ortiz, V. Budamagunta, J. H. Elisseeff, J. Campisi, M. Almeida, G. Zheng and D. Zhou, *Nat. Commun.*, 2020, **11**, 1996.
- 25 X. Zhang, D. Thummuri, X. Liu, W. Hu, P. Zhang, S. Khan, Y. Yuan, D. Zhou and G. Zheng, *Eur. J. Med. Chem.*, 2020, **192**, 112186.
- 26 P. Pal, D. Thummuri, D. Lv, X. Liu, P. Zhang, W. Hu, S. K. Poddar, N. Hua, S. Khan, Y. Yuan, X. Zhang, D. Zhou and G. Zheng, *J. Med. Chem.*, 2021, **64**, 14230–14246.
- 27 S. Zhang, Y. Chen, Z. Xu, J. Yang, R. Sun, J. Wang, Y. Sun, B. Jiang, X. Yang and W. Tan, *Theranostics*, 2022, **12**, 7476–7490.
- 28 X. Zhang, Y. Tao, Z. Xu, B. Jiang, X. Yang, T. Huang and W. Tan, *Biochem. Pharmacol.*, 2024, **230**, 116542.
- 29 P. Zhang, X. Zhang, X. Liu, S. Khan, D. Zhou and G. Zheng, *Explor. Target. Antitumor Ther.*, 2020, **1**, 259–272.
- 30 A. J. Souers, J. D. Levenson, E. R. Boghaert, S. L. Ackler, N. D. Catron, J. Chen, B. D. Dayton, H. Ding, S. H. Enschede, W. J. Fairbrother, D. C. Huang, S. G. Hymowitz, S. Jin, S. L. Khaw, P. J. Kovar, L. T. Lam, J. Lee, H. L. Maecker, K. C. Marsh, K. D. Mason, M. J. Mitten, P. M. Nimmer, A. Oleksijew, C. H. Park, C. M. Park, D. C. Phillips, A. W. Roberts, D. Sampath, J. F. Seymour, M. L. Smith, G. M. Sullivan, S. K. Tahir, C. Tse, M. D. Wendt, Y. Xiao, J. C. Xue, H. Zhang, R. A. Humerickhouse, S. H. Rosenberg and S. W. Elmore, *Nat. Med.*, 2013, **19**, 202–208.
- 31 M. S. Gadd, A. Testa, X. Lucas, K. Chan, W. Chen, D. J. Lamont, M. Zengerle and A. Ciulli, *Nat. Chem. Biol.*, 2017, **13**, 514–521.
- 32 R. I. Troup, C. Fallan and M. G. J. Baud, *Explor. Target Antitumor Ther.*, 2020, **1**, 273–312.
- 33 A. Zagidullin, V. Milyukov, A. Rizvanov and E. Bulatov, *Explor. Target Antitumor Ther.*, 2020, **1**, 381–390.
- 34 Y. Dong, T. Ma, T. Xu, Z. Feng, Y. Li, L. Song, X. Yao, C. R. Ashby and G. Hao, *Acta Pharm. Sin. B*, 2024, **14**, 4266–4295.
- 35 N. A. Zografou-Barredo, A. J. Hallatt, J. Goujon-Ricci and C. Cano, *Bioorg. Med. Chem.*, 2023, **88–89**, 117334.
- 36 M. Hoffmann, C. Kasserra, J. Reyes, P. Schafer, J. Kosek, L. Capone, A. Parton, H. Kim-Kang, S. Surapaneni and G. Kumar, *Cancer Chemother. Pharmacol.*, 2013, **71**, 489–501.
- 37 A. Bricelj, C. Steinebach, R. Kuchta, M. Gütschow and I. Sosič, *Front. Chem.*, 2021, **9**, 707317.
- 38 J. Davila, A. Chassepot, J. Longo, F. Boulmedais, A. Reisch, B. Frisch, F. Meyer, J. Voegel, P. J. Mesini, B. Senger, M. Metz-Boutigue, J. Hemmerle, P. Lavalle, P. Schaaf and L. Jierry, *J. Am. Chem. Soc.*, 2012, **134**, 83–86.
- 39 P. Cheol-Min, M. Bruncko, J. Adickes, J. Bauch, H. Ding, A. Kunzer, K. C. Marsh, P. Nimmer, A. R. Shoemaker, X. Song, S. K. Tahir, C. Tse, X. Wang, M. D. Wendt, X. Yang, H. Zhang, S. W. Fesik, S. H. Rosenberg and S. W. Elmore, *J. Med. Chem.*, 2008, **51**, 6902–6915.
- 40 G. Zheng, D. Zhou, W. Hu, D. Thummuri, P. Zhang, P. Pratik, D. Lv and Y. Yuan, WO2023107606A1, 2023.
- 41 A. P. Crew, K. R. Hornberger, J. Wang, H. Dong, M. Berlin and C. M. Crews, WO2019195609A2, 2019.
- 42 S. Khan, P. Kellish, N. Connis, D. Thummuri, J. Wiegand, P. Zhang, X. Zhang, V. Budamagunta, N. Hua, Y. Yang, U. De, L. Jin, W. Zhang, G. Zheng, R. Hromas, C. Hann, M. Zajack-Kaye, F. J. Kaye and D. Zhou, *Cell Death Discovery*, 2023, **9**, 1.

